Organic Geochemistry 218 (2026) 105139

Contents lists available at ScienceDirect

Organic Geochemistry

journal homepage: www.elsevier.com/locate/orggeochem

Improved procedures for the cleavage and reduction of GDGTs for hydrogen isotope analysis

C.D. Rosendahl [a,*], X. Zhao [a], A.E. Maloney [b], J.M. McFarlin [c], K.J. Keller [d], R. Kreutz [e], J. Altun [e], L.H. Bachmann [a], J. Hartmann [a], H.K. Batther [b], A.N. Calhoun [d], M. Elvert [e,f], A. Pearson [d], W.D. Leavitt [g,h], S.H. Kopf [b], F.J. Elling [a,*]

[a] Leibniz-Laboratory for Radiometric Dating and Isotope Research, Christian-Albrecht University of Kiel, Kiel 24118, Germany
[b] Department of Geological Sciences, University of Colorado Boulder, Boulder, CO, United States
[c] Department of Geology and Geophysics, University of Wyoming, Laramie, WY, United States
[d] Department of Earth and Planetary Sciences, Harvard University, Cambridge, MA 02138, United States
[e] MARUM-Center for Marine Environmental Sciences, University of Bremen, Germany
[f] Faculty of Geosciences, University of Bremen, Germany
[g] Department of Geology & Geophysics, University of Utah, Salt Lake City, UT 84112, United States
[h] Department of Earth Sciences, Dartmouth College, Hanover, NH 03755, United States

ARTICLE INFO

Associate editor: Cindy de Jonge

Keywords:
GDGT
Hydrogen isotopes
Thaumarchaeota
Nitrososphaeria
Ether cleavage
Hydrogenation

ABSTRACT

Glycerol dialkyl glycerol tetraether (GDGT) membrane lipids of archaea and bacteria are commonly used to reconstruct past environmental conditions, mainly temperature and pH, based on their relative abundances. In contrast, the stable hydrogen isotope composition (δ^2H) of GDGTs has received comparatively little attention, although it may hold additional paleoenvironmental information. Established methods for the analysis of δ^2H require chemical degradation into the constituent alkyl chains via cleavage of the ether bonds of GDGTs and reduction of the halogenated alkyl chains. Two of these GDGT cleavage and reduction methods have been widely used but never been compared: 1) boron tribromide (BBr_3) and lithium triethylborohydride (SH), and 2) hydroiodic acid (HI) and platinum oxide (PtO_2) combined with H_2. Here, we compare combinations of these cleavage and reduction methods in terms of yield, recovery, reproducibility, and hydrogen isotopic fractionation to provide improved protocols. Based on our experiments, for archaeal GDGTs we recommend ether cleavage with non-stabilized HI for 4 h at 120 °C followed by hydrogenation with SH for 2 h at 60 °C for optimal efficiency and minimized hydrogen isotopic fractionation. For bacterial GDGTs, we recommend the same cleavage protocol but hydrogenation with PtO_2 and H_2, as it was not possible to implement a reliable SH isotope fractionation correction for these biomarkers. The improvement of these ether cleavage and hydrogenation protocols represents an important step in the development of δ^2H of GDGTs as a possible paleoenvironmental proxy and will improve the comparability of future paleorecords using δ^2H derived from GDGTs.

1. Introduction

The glycerol dialkyl glycerol tetraether (GDGT) membrane lipids of archaea and bacteria are commonly used for paleoenvironmental reconstructions (Schouten et al., 2013). Their application has been primarily limited to reconstructions of temperature and pH from ocean and lake sediments, soils, and other systems. Such reconstructions typically rely on the quantification of the relative abundances of GDGTs. However, GDGTs may also contain paleoenvironmental information encoded in their isotopic compositions.

The carbon isotopic composition ($\delta^{13}C$) of archaeal (isoprenoid) GDGTs has been routinely studied to yield insights into the sources of GDGTs in modern systems and in paleoenvironments (Hoefs et al., 1997; Summons et al., 1998; Kuypers et al., 2001; Pearson et al., 2016; Hurley et al., 2019; Blewett et al., 2022). The $\delta^{13}C$ of archaeal GDGTs found in marine sediments reflects the composition of the dissolved inorganic carbon from the water column due to the autotrophic metabolism of their dominant producers, planktonic Thaumarchaeota (Hoefs et al.,

* Corresponding authors at: Leibniz-Laboratory for Radiometric Dating and Isotope Research, Christian-Albrecht University of Kiel, Postfach 50, Max-Eyth-Str. 11-13, 24118 Kiel, Germany.
E-mail addresses: crosendahl@leibniz.uni-kiel.de (C.D. Rosendahl), felling@leibniz.uni-kiel.de (F.J. Elling).

https://doi.org/10.1016/j.orggeochem.2026.105139
Received 23 October 2025; Received in revised form 21 January 2026; Accepted 25 January 2026
Available online 5 February 2026

1997; Könneke et al., 2012; Pearson et al., 2016), now the class *Nitrososphaeria* in the phylum *Thermoproteota* (Oren and Garrity, 2021). Further, it has been suggested that the carbon isotopic fractionation in GDGTs of *Nitrososphaeria* depends on growth rate and dissolved CO_2 concentration, suggesting a potential application as a pCO_2 paleobarometer (Hurley et al., 2019; Pearson et al., 2019; He et al., 2022). Carbon isotopic compositions of GDGTs have also been used to constrain their sources (Zhang et al., 2011; Pearson et al., 2016; Polik et al., 2018; Keller et al., 2025a), which improves the interpretability of other GDGT-based proxies such as the TEX_{86} paleothermometer. Similarly, the $\delta^{13}C$ of bacterial branched GDGTs has been used to constrain the sources of GDGTs used in the MBT/CBT proxies for past continental or lake temperatures (Weijers et al., 2010; Colcord et al., 2017; Weber et al., 2018; Elling et al., 2023).

In contrast to $\delta^{13}C$, the stable hydrogen isotopic composition (δ^2H) of GDGTs has only recently been studied in detail. These studies suggest that the δ^2H of archaeal isoprenoid GDGTs may serve as a paleohydrological proxy (e.g. Leavitt et al., 2023; Harris et al., 2025; Keller et al., 2025b). Specifically, *Nitrososphaeria* incorporate H primarily from water due to their autotrophic metabolism (Leavitt et al., 2023). Further, the δ^2H of GDGTs from archaea shows minimal sensitivity to growth rate, in contrast to bacteria and eukaryotes (Leavitt et al., 2023). Even outside of *Nitrososphaeria*, δ^2H of lipids of heterotrophic and autotrophic archaea is primarily dependent on the δ^2H of growth water and shows a limited range of variability compared to bacteria and eukaryotes (Dirghangi and Pagani, 2013; Rhim et al., 2023; Harris et al., 2025). Therefore, GDGTs derived from *Nitrososphaeria* and potentially other archaea should primarily reflect the composition of their growth water, enabling their use as a paleohydrological proxy.

The δ^2H analyses of GDGTs are currently mostly performed using gas chromatography coupled to pyrolysis isotope ratio mass spectrometry (GC-P-IRMS) after chemical degradation (Kaneko et al., 2011), although a method for the analysis of δ^2H of intact GDGTs using a customized high-temperature GC-P-IRMS system has been recently been established (Lengger et al., 2021). In order to make GDGTs amenable to conventional GC-P-IRMS analysis, these large molecules (C_{86}) must be converted into their constitutive alkyl or biphytanyl chains (C_{40}) by cleavage of the ether bonds. There are three established GDGT cleavage and reduction methods: 1) using boron tribromide (BBr_3) for ether cleavage and lithium triethylborohydride (Superhydride, SH) for reduction of the alkyl bromides resulting from ether cleavage (Summons et al., 1998; Jahn et al., 2004), 2) using hydroiodic acid (HI) for ether cleavage and platinum oxide combined with hydrogen ($PtO_2 + H_2$) for reduction of the alkyl iodides resulting from cleavage (Kaneko et al., 2011), and 3) also using HI for ether cleavage but lithium aluminium hydride ($LiAlH_4$) for reduction (Hoefs et al., 1997). This method, using HI and $LiAlH_4$, had been used regularly in the 2000s and early 2010s (Pancost et al., 2000; Pearson et al., 2004; Weijers et al., 2010). The reduction of the alkyl iodides is achieved by the preferential exchange (Kaneko et al., 2011) of the alkyl bromide or iodide with hydrogen, subsequently also referred to as hydrogenation. Comparison of $PtO_2 + H_2$ and $LiAlH_4$ by Lengger et al. (2014) showed up to 2.8-times higher yields (avg. 1.9-times) using $PtO_2 + H_2$, probably caused by the two required column separations after the $LiAlH_4$ treatment. Therefore, we excluded this method from our study. The other two methods (BBr_3 & SH, HI & $PtO_2 + H_2$) have been modified and also used widely since their initial publication (e.g. Liu et al., 2016; Leavitt et al., 2023; Zhu et al., 2024; Harris et al., 2025), but they have never been compared in terms of yield, recovery or reproducibility. Further, the BBr_3 and SH method has not been tested for isotopic fractionation effects, in this case hydrogen isotopic fractionation.

In order to determine the optimal procedure for the routine preparation of GDGTs for δ^2H analysis, existing protocols have to be evaluated and improved in terms of yield, efficiency, and hydrogen isotope fractionation. Therefore, we compared the two currently used cleavage and reduction protocols and tested multiple reaction conditions and combinations to find the optimal procedure for the cleavage and reduction of GDGTs for hydrogen isotope analysis.

2. Material & methods

In order to identify the optimal cleavage and reduction procedure for subsequent hydrogen isotope analysis, 4 major experiments (Fig. 1) were conducted: 1) Optimization of HI ether cleavage efficiency, 2) Recovery comparison of HI vs. BBr_3 and SH vs. $PtO_2 + H_2$, 3) Optimization of SH hydrogenation, 4) Comparison of the hydrogen isotope fractionation during hydrogenation with SH and PtO_2.

Additionally, we compared the recovery after cleavage with stabilized versus non-stabilized HI, both fresh and 4 months after first opening the reagent in order to evaluate the long-term usability of laboratory stocks of HI.

Since we did not compare different brands of the used reagents, we provide a list of reagents used for our experiments (Supplementary information: Table S1).

2.1. Optimization of HI ether cleavage efficiency

In 2022, the efficiency of HI ether cleavage depending on temperature, time, sample quantity and type of HI was tested at University of Colorado Boulder. This marked the starting point (Fig. 1) of our research to optimize the GDGT cleavage and reduction protocol. To assess HI ether cleavage efficiency, 24 glass vials (2 mL with PTFE-Si-PTFE septa caps) containing 1:1 hexadecyl ether ($C_{16}OC_{16}$) standard and squalane standard (10 μg and 50 μg each) were split into two 12-sample batches (Table 1) and cleaved with non-stabilized HI (57% w/w aq. solution) or in the other case with stabilized HI (57% w/w aq. solution stabilized with 1.5% hypophosphorus acid; Supplementary information: Table S1). First, 500 μL of the respective HI was added to each sample and both the cap and the vial headspace were purged with N_2 before closing the caps tightly. The closed vials of both batches were kept in pre-heated heating blocks at either 70 °C for 16 h, 120 °C for 4 h or 120 °C for 12 h (Table 1). Afterwards, the samples were extracted by liquid–liquid extraction with hexane (See Supplementary Information: HI-SH protocol) and subsequently the iodinated C_{16} and $C_{16}OC_{16}$ were quantified using Gas Chromatography coupled to Flame Ionization Detection (GC-FID; See section 2.6.1).

In accordance with the results of the recovery comparison of HI/BBr_3 and SH/PtO_2 (See section 3.2, Fig. 3) that showed about twice the recovery using HI compared to BBr_3, we decided not to conduct any similar optimization attempts for BBr_3.

2.2. Recovery comparison of HI vs. BBr_3 and SH vs. PtO_2

This test compared the GDGT recovery of the two established GDGT cleavage and reduction methods: 1) modified from Summons et al. (1998) with BBr_3 and SH, and 2) modified from Kaneko et al. (2011) with HI and $PtO_2 + H_2$. Therefore, 12 samples, each containing 5% hydrolysed total lipid extract (TLE) obtained from ~30 mg homogenised *Sulfolobus acidocaldarius* biomass (See Supplementary information for cultivation and acid hydrolysis procedures) and 50 μg squalane standard were treated with HI or BBr_3 and SH or $PtO_2 + H_2$ in different combinations (Table 2). We decided to use *S. acidocaldarius* biomass as it is easier to grow in large amounts than *Nitrososphaeria* and its lipid composition (predominantly GDGT-1 through -4) is more similar to the biomass of *Nitrososphaeria* than available commercial standards, e.g., $C_{16}OC_{16}$, and thus should provide more realistic information on the efficiency of these methods regarding archaeal GDGTs.

Samples that were cleaved with HI were kept at 120 °C for 4 h in accordance with the results of the HI optimization test, whereas the BBr_3 samples were kept at 60 °C for 2 h (Summons et al., 1998). The cleaved samples were reduced with either SH at 60 °C for 2 h or with PtO_2 in hexane and H_2 bubbling for 90 min. Afterwards, the SH samples were extracted by liquid–liquid extraction with hexane and the PtO_2 samples

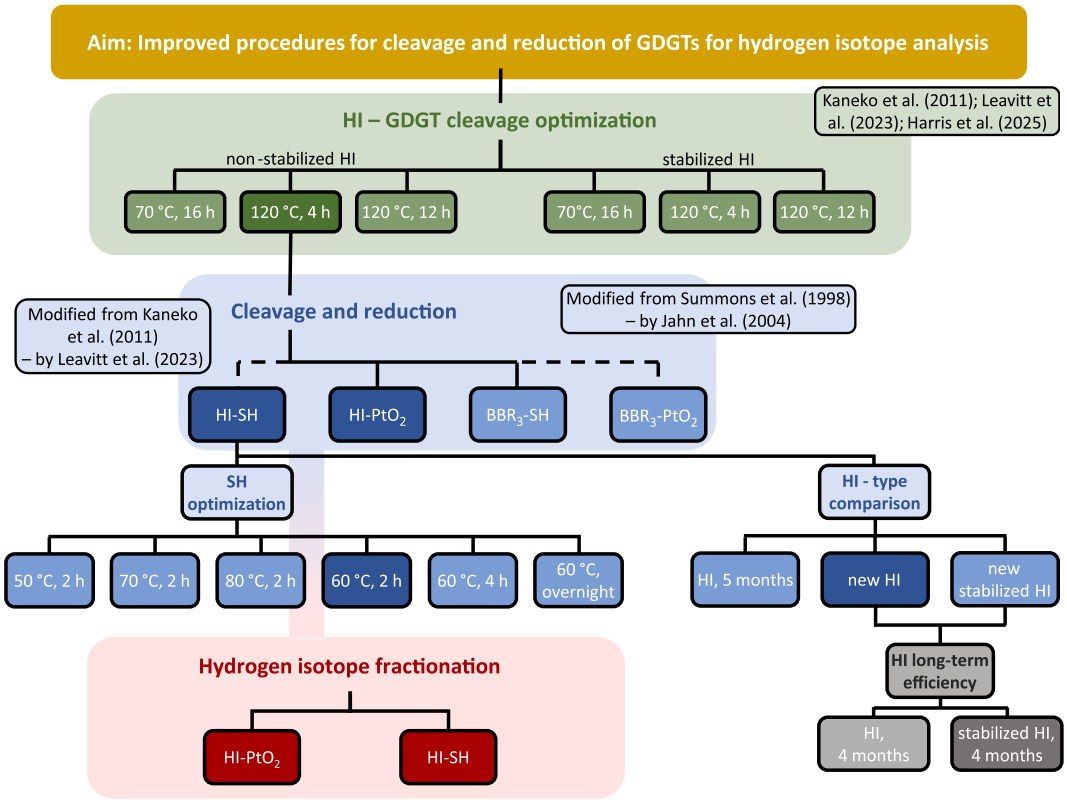

Fig. 1. Schematic overview of the development of the improved procedure for cleavage and reduction of GDGTs for hydrogen isotope analysis. The HI assays displayed in green mark the starting point of this research, performed at University of Colorado Boulder, in order to optimize the sample recovery of the HI cleavage procedure (See section 2.1). The experiments displayed in blue and the additional HI long-term efficiency test (grey) were conducted at University of Kiel and investigate the sample recovery (See sections 2.2; 2.3; 2.4). The isotope fractionation investigation following the recovery experiments is displayed in red and was performed as a joint project at University of Kiel and University of Colorado Boulder (See section 2.5). Dark colour shading marks the favoured cleavage/hydrogenation procedures/conditions compared to the other tested parameters (light colour shading). The dashed line in the "cleavage and reduction" section represents combinations of the two existing cleavage and reduction protocols by Summons et al. (1998) and Kaneko et al. (2011). (For interpretation of the references to colour in this figure legend, the reader is referred to the web version of this article.)

Table 1
Overview of the reaction conditions of the HI ether cleavage efficiency test.

Type of HI	Temperature & Time	$C_{16}OC_{16}$ [µg]	Replicates	Total samples
non-stabilized	70 °C, 16 h	10; 50	2	4
	120 °C, 4 h	10; 50	2	4
	120 °C, 12 h	10; 50	2	4
stabilized	70 °C, 16 h	10; 50	2	4
	120 °C, 4 h	10; 50	2	4
	120 °C, 12 h	10; 50	2	4

Table 2
Overview of the reaction conditions of the comparison of HI vs. BBr_3 and SH vs. $PtO_2 + H_2$.

Method	Cleavage	Reduction / Hydrogenation	Replicates
HI + SH	HI: 120 °C, 4 h	SH: 60 °C, 2 h	3
HI + PtO_2	HI: 120 °C, 4 h	$PtO_2 + H_2$: 90 min	3
BBr_3 + SH	BBr_3: 60 °C, 2 h	SH: 60 °C, 2 h	3
BBr_3 + PtO_2	BBr_3: 60 °C, 2 h	$PtO_2 + H_2$: 90 min	3

were filtered using Pasteur pipettes filled with combusted glass wool. The obtained biphytanes (BP) were quantified using GC-FID. The detailed protocols can be found in the SI.

2.3. Recovery optimization of SH hydrogenation

In accordance with the results of the recovery comparison of HI/BBr_3 and SH/PtO_2 (Section 3.2), we decided to further optimize only the HI-SH method, as it showed the best recovery by a large margin and has benefits in handling and safety compared to working with BBr_3 and H_2 (See section 3.2). In order to optimize the hydrogenation with SH, 18 samples, each containing 2.5% hydrolysed TLE of ~15 mg homogenised *S. acidocaldarius* biomass and 50 µg squalane standard, were cleaved with HI at 120 °C for 4 h and subsequently hydrogenated with SH at 6 different temperature–time combinations as triplicates. Since in many previous research papers SH hydrogenation was performed at 60 °C or 70 °C for 2 h (Jahn et al., 2004; Liu et al., 2012, 2016; Guan et al., 2016), we tested the following temperature/time combinations: 50 °C, 60 °C, 70 °C and 80 °C for 2 h and 60 °C for 4 h and overnight (19 h). The samples were again extracted by liquid–liquid extraction with hexane (See Supplementary information: HI-SH protocol) and the obtained biphytanes were quantified using GC-FID (See section 2.6.1).

2.4. Comparison of stabilized vs. non-stabilized HI

In terms of long-term usability of laboratory stocks of HI, which may degrade in contact with O_2 and light (Husa and Shattuck, 1932), we decided to investigate the ether cleavage efficiency of non-stabilized HI compared to stabilized HI. First, we compared the recovery using freshly opened non-stabilized HI versus freshly opened stabilized HI (Supplementary information: Table S1) versus 5-months-old non-stabilized HI. After each use of the HI, the headspace of the reagent bottles is flushed with N_2 before sealing. After 4 months we repeated the test with the now aged non-stabilized and stabilized HI. All tests were performed in triplicate and the reagents were stored at 4 °C in the dark. Each replicate sample contained 2.5% of hydrolysed TLE of ~15 mg homogenised *S. acidocaldarius* biomass and 50 μg squalane standard. In accordance with the results of experiments 3.1 and 3.3, the GDGTs were cleaved with the respective HI at 120 °C for 4 h, hydrogenated with SH at 60 °C for 2 h and the obtained biphytanes were subsequently measured using GC-FID (see section 2.6.1).

2.5. Comparison of the hydrogen isotope fraction during hydrogenation with SH and PtO_2

In the case of hydrogen isotope analysis of GDGTs, it is important that the processing of the samples introduces minimal isotopic fractionation or at least a consistent and highly reproducible fractionation which can be corrected for. We chose the two GDGT cleavage and reduction methods with the highest recovery rates, HI-SH and HI-PtO_2, to investigate their isotopic fractionation. Therefore, after cleavage of the biomass of *S. acidocaldarius* and *Solibacter usitatus* with HI for 4 h at 120 °C (See Supplementary Information), SH and PtO_2 hydrogenation tests were conducted, with each 4 replicates spiked with squalane and several measurements (Supplementary information data table), in order to investigate hydrogen isotope fractionation effects on branched GDGTs and isoprenoid GDGTs. As these tests showed different isotope fractionation for the hydrogenation with SH, the SH and PtO_2 test was repeated with squalane, octadecyl ether ($C_{18}OC_{18}$) and an *n*-alkane standard mix containing C_8 to C_{40} (Supelco, 40147-U), whereby 22 alkanes (C_{19} to C_{40}) were interpreted. Additional SH hydrogenation tests were conducted in order to investigate possible aging effects of SH. Therefore, 8 replicate samples, each containing 10 μg of iodinated C_{18} (C_{18}i), iodinated C_{34} (C_{34}i), and squalane, were hydrogenated with either freshly opened SH or 4-month-old SH.

In accordance with the protocols of the HI/BBr_3 and SH/PtO_2 recovery tests (Supplementary information) and the results of the SH optimization test (see sections 3.2 and 3.3), the hydrogenation with SH was performed at 60 °C for 2 h, whereas the hydrogenation with PtO_2 in hexane and H_2 bubbling was carried out for 90 min. After liquid–liquid extraction of the SH samples and filtration of the PtO_2 samples, respectively, the hydrogen isotopic composition of the samples was measured GC-P-IRMS (See section 2.6.2). As part of these tests, a hydrogen isotope fractionation correction for the hydrogenation step with SH was developed (see section 2.6.2) – similar to the H_2 correction which was established for the PtO_2 hydrogenation by Leavitt et al. (2023).

2.6. Analysis and data processing

2.6.1. GC-FID analyses

The GC-FID analysis of experiment 2.1 was performed using a Trace 1310 gas chromatograph coupled to a flame ionization detector (FID; ThermoFisher Scientific) and equipped with a split-splitless injector (analyses performed in splitless mode) and an Agilent DB5-HT column (30 m x 250 μm inner diameter (ID), 0.1 μm film thickness). All samples were dissolved in hexane. The carrier gas Helium (He) was set to a constant flow rate of 1.2 mL/min. The injection volume was 1 μL. The initial oven temperature of 40 °C was held for 2 min and subsequently increased at a rate of 20 °C/min to 120 °C, followed by a second ramp of 15 °C/min until reaching 345 °C with a holding time of 7 min. The peak areas of iodinated C_{16} and $C_{16}OC_{16}$ (See section 2.1) were normalized to the peak area of squalane for each sample and the relative proportion of the squalane normalized peak areas of iodinated C_{16} and $C_{16}OC_{16}$ in relation to the initial, squalane normalized peak area of $C_{16}OC_{16}$ of the untreated sample was determined. The relative proportions of each duplicate set for each tested parameter were averaged and the standard deviation was determined using Gaussian error propagation.

The GC-FID analysis of experiment 2.2 was performed using a ThermoFisher Scientific Focus GC-FID equipped with a Restek RXI-5 ms capillary column (60 m x 320 μm (ID) x 0.25 μm film thickness). All samples were dissolved in hexane. Nitrogen (N_2) was used as the carrier gas at a constant pressure of 200 kPa. The initial oven temperature was set to 70 °C. Following the injection of 2 μL sample volume, the initial temperature of 70 °C was hold for 2 min. After holding, a first ramp of 25 °C/min was applied until reaching 250 °C, followed by a second ramping with 3 °C/min until reaching 310 °C, which was held for 35 min.

In terms of the experiment 2.3 the GC-FID analysis was performed using an Agilent 6890 GC-FID equipped with a Restek RTX-200 capillary column (30.0 m × 320 μm (ID) × 0.25 μm film thickness). All samples were dissolved in hexane. The carrier gas H_2 was set to a constant pressure of 44.0 kPa, a flow rate of 2.7 mL/min, and an average linear velocity of 50 cm/sec and the initial oven temperature was set to 50 °C. Following the injection of 1 μL sample volume, the temperature was increased at a rate of 10 °C/min to 150 °C, where the temperature was held for 5 min. A second ramp of 5 °C/min was applied until reaching 330 °C, which was held for 20 min.

The GC-FID analysis of experiment 2.4 was performed using a ThermoFisher Scientific Trace 1610 GC-FID equipped with a Restek RXI-5 ms capillary column (30 m x 250 μm (ID) x 0.25 μm film thickness). All samples were dissolved in hexane. The carrier gas (He) was set to a constant flow rate of 1.2 mL/min. Following the injection of 1 μL sample volume, the initial oven temperature of 60 °C was held for 1 min and subsequently increased at a rate of 10 °C/min to 150 °C. A second ramp of 4 °C/min was applied until reaching 310 °C with a holding time of 20 min.

All analyses were performed in splitless mode. Since the squalane-spiked samples showed a large variability in their peak area, an external standard curve with sample matching standard concentrations was measured repeatedly to ensure stable measurements and a high precision.

The peak areas of the biphytanes (experiments 2.2, 2.3 and 2.4) were normalized to the peak area of squalane for each sample. The peak areas of each triplicate set for each tested parameter were averaged and the standard deviations determined. For each experiment, the averaged peak areas were compared with each other and displayed as the relative proportion of the tested parameter with the highest peak area. The standard deviation was determined using Gaussian error propagation. In terms of quality control of the data, the BP0/BP1 ratio and BP1/BP2 ratio were calculated and were constant throughout each type of experiment. Outliers were identified using a Q-test with 90% confidence interval and removed from subsequent analyses.

2.6.2. GC-P-IRMS analysis

The hydrogen isotope analysis with GC-P-IRMS (see section 2.5) was performed using a GC IsoLink II IRMS System (ThermoFisher Scientific) and was followed by extensive data processing. The GC IsoLink II IRMS System consisted of a Trace 1310 GC with a programmable temperature vaporization (PTV) injector and an Agilent DB5-HT column (30 m × 0.25 mm and 10 μm film thickness), delivering the sample to the Isolink II, followed by a ConFlo IV interface to the 253 Plus mass spectrometer (Thermo Fisher Scientific) at the Department of Geological Sciences, University of Colorado, Boulder. The reactor temperature was 1420 °C. Following the injection of 3–8 μL sample volume (equalling 100–150 ng biphytane per injection), the sample was transferred to the GC column using a fast ramp of 12 °C/min from 40 °C to 450 °C, which was held for 6 min, and a constant carrier flow rate of 1.2 mL/min Helium. After an initial hold of the GC oven at 40 °C for 1 min, the temperature was

increased to 120 °C at a rate of 20 °C/min and further ramped with 15 °C/min to 345 °C, and subsequently held for 5 min.

The data was calibrated and corrected following the approach described in Keller et al. (2025) and detailed hereafter: The hydrogen isotopic composition is displayed using the delta notation (δ; in ‰) relative to the international seawater standard on the VSMOW-SLAP (Vienna Standard Mean Ocean Water, Standard Light Antarctic Precipitation) scale and all ^{2}H/1H fractionation factors are reported in epsilon notation (ε^2H; in ‰):

$$\delta^2H = \delta D = \frac{\left(\frac{^2H}{^1H}\right)_{sample} - \left(\frac{^2H}{^1H}\right)_{standard}}{\left(\frac{^2H}{^1H}\right)_{standard}} \cdot 1000 \quad (1)$$

$$\varepsilon^2H = \left(\frac{\delta^2H_{hydrogenated} + 1000}{\delta^2H_{initial} + 1000} - 1\right) \cdot 1000 \quad (2)$$

The δ^2H was initially determined relative to the H_2 laboratory reference gas (δ^2H_{raw}), and subsequently calibrated externally. Therefore, a standard n-alkane mixture (A7; *n*C_{16}-*n*C_{30}; Arndt Schimmelmann, Indiana University; values updated September 2024) combined with a C_{36} n-alkane standard (nC_{36}; −259.2 ± 1.3‰ vs. VSMOW; Arndt Schimmelmann, Indiana University) were analysed repeatedly at regular intervals among the samples. The calibration was carried out in the R statistical environment using 6211 compound-specific measurements from 475 analyses of the combined standard and comprises correction of the data for background, scale compression and peak-size effects (Eq. (3)).

$$\delta_x = \frac{A_{peak}}{A_{peak} - A_{bgrd}} \cdot \left(\delta_{H_2} + \delta_{peak/H_2} + \delta_{H_2} \cdot \delta_{peak/H_2}\right) - \frac{A_{peak}}{A_{peak} - A_{bgrd}} \cdot \delta_{bgrd} \quad (3)$$

Peak areas are reported in volt-seconds (Vs), represent time-integrated peak amplitudes after baseline subtraction, are H3 factor corrected and range from 3.0 to 50.0 Vs (Fig. S2). The H3 factor was determined daily using the default method. The analyte peaks were integrated in the Isodat software (v 3.0, Thermo Scientific), with a mixture of automatic processing and manual correction of the peak boundaries and integration. Each chromatogram was manually checked for misinjections, any contaminates introduced during sample preparation, retention time outliers, peak interference due to co-elution and background correction before and after the eluting analyte peak. Analysis by Leavitt et al. (2023) suggested integration errors to be negligible. The reference gas (δ_{H2}) value was derived from the standard measurements and estimated based on the approach of Polissar and D'Andrea, (2014). Two different hydrogen tanks have been used throughout the analyses: i) tank 1 (2023 – 2024) had a δ_{H2} of 310.2 ± 2.1‰ and ii) tank 2 (2025) had a δ_{H2} of 260.0 ± 3.4. The uncertainty estimates for individual analyte δ^2H values were defined conservatively by selecting the largest of the following three metrics: i) the propagated calibration uncertainty (1.0‰ to 2.5‰), ii) the bias-corrected pooled standard deviation of the samples (1.0‰ to 5.0‰) or iii) the bias-corrected standard deviation of the nC_{36} standard (4.3‰). The bias-correction and standard deviation pooling was conducted following the approach of Polissar and D'Andrea (2014).

Additionally, analyte δ^2H values were corrected for the addition of H during the alkyl iodide hydrogenation. The applied hydrogenation correction depended on the hydrogenation method as the SH hydrogenation treatment caused unexpected isotopic fractionation effects. Samples treated with PtO_2 and H_2 gassing were corrected as described in Leavitt et al. (2023) using a long-term estimated δ^2H (based on internal measurements at CU Boulder) of −676 ± 134‰ for the added H. The details, differences and as the result modifications of the hydrogenation correction protocol for SH treated samples are discussed in more detail in the results (See section 3.5).

3. Results and discussion

3.1. Optimization of HI ether cleavage efficiency

The efficiency of HI for ether cleavage (examined using $C_{16}OC_{16}$) was tested as a factor of temperature, time, sample quantity and type of HI. The results (Fig. 2) show varying efficiency and thus the importance of choosing the optimal reaction parameters. The highest degree of ether cleavage, calculated as the relative proportion of iodinated C_{16} compared to the sum of iodinated C_{16} and residual $C_{16}OC_{16}$ both normalized to the starting C_{16}-Squalane ratio, was achieved at 120 °C with an efficiency of more than 80% for 13 of 16 assays. Cleavage at 70 °C was not sufficient despite the longer experiment time (16 h), with proportions between 15.4% and 65.2%, but mainly below 50%. A reaction time of 4 h or 12 h at 120 °C yielded an efficiency of 69.5% to 100% respectively, for both 10 μg and 50 μg samples. However, the 10 μg samples with 12 h reaction time show a greater average loss of material of 20.3% compared to 0.9% at 4 h reaction time. The material loss was calculated as the percental difference of the sum of iodinated C_{16} and residual $C_{16}OC_{16}$ to the initial amount of $C_{16}OC_{16}$, normalized to the starting C_{16}-Squalane ratio. In order to minimize the risk of material loss and in terms of economy of time and improved workflow with regard to the subsequent steps, we recommend 4 h of HI treatment. If the sample volume is very small, it is possible to use longer reaction times in order to obtain as much cleaved biomass as possible, but possible material loss due to evaporation and leaking of the sample vials may need to be considered. Future attempts to improve the workflow might include testing for even shorter HI reaction times, however, higher temperatures are not applicable as the boiling point of HI (usually commercially available with 57% w/w) is reached at 127 °C.

The comparison of non-stabilized versus stabilized HI indicates a small advantage of using non-stabilized HI, but further tests with more replicates may be needed. When used in excess, HI does not seem to have a significant influence on ether cleavage efficiency (See section 3.4). Nevertheless, it is important to note that different brands of HI were used for these two sets of tests.

3.2. Recovery comparison of HI vs. BBr_3 and SH vs. PtO_2

The results of the recovery test of the HI-SH, BBr_3-SH, HI-PtO_2 and BBr_3-PtO_2 cleavage and hydrogenation protocol combinations (examined using *S. acidocaldarius* biomass) are displayed as the relative amount of recovered material in percent compared to the assay with the highest amount of recovered material (Fig. 3). The data show that all biphytanes (BP), regardless of the number of incorporated cyclopentane rings (indicated by the number, i.e., BP0 = 0 rings, BP1 = 1 ring, etc.), are recovered similarly within one protocol. However, the recoveries of BPs differ depending on cleavage and hydrogenation methods, with the HI-SH protocol resulting in the highest recovery compared to HI-PtO_2 (ca. 67%), BBr_3-SH (ca. 49%) and BBr_3-PtO_2 (ca. 6%). The HI-SH protocol has further advantages as the handling of these reagents eliminates some safety concerns such as the high toxicity of BBr_3 and the risk of forming explosive gas mixtures with continuous flow of H_2. Additionally, hydrogenation with SH causes less scattering regarding the isotopic fractionation than hydrogenation with PtO_2 and H_2 (Section 3.5). Since the recovery rate of both BBr_3 assays was less than 50% of the HI assays and because of the safety disadvantages, we decided to not further test and optimize the BBr_3 cleavage protocol.

The relative recovery compared to the starting material cannot be determined as the different GDGTs, due to their chemical structure with varying cyclopentane ring combinations, contribute differently to multiple types of biphytanes. This cannot be predicted and corrected for without prior chromatographic isolation of individual GDGTs. If such information is desired, future studies could isolate individual GDGTs using preparative high performance liquid chromatography followed by ether cleavage and hydrogenation. Moreover, the abundance of GDGTs

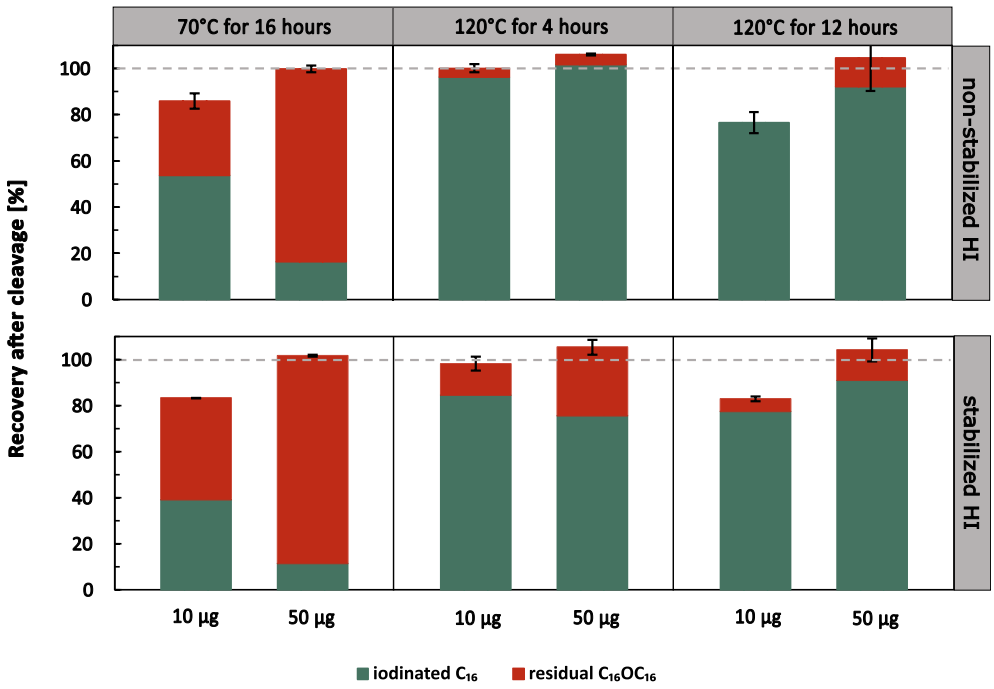

Fig. 2. Relative proportion [%] of iodinated C_{16} (green) after the ether cleavage of $C_{16}OC_{16}$ with non-stabilized HI or stabilized HI at various reaction conditions (Column 1: 70 °C for 16 h; Column 2: 120 °C for 4 h, Column 3: 120 °C for 12 h) – compared to the remaining $C_{16}OC_{16}$ (red) The data are normalized to the starting C_{16}-Squalane ratio. (For interpretation of the references to colour in this figure legend, the reader is referred to the web version of this article.)

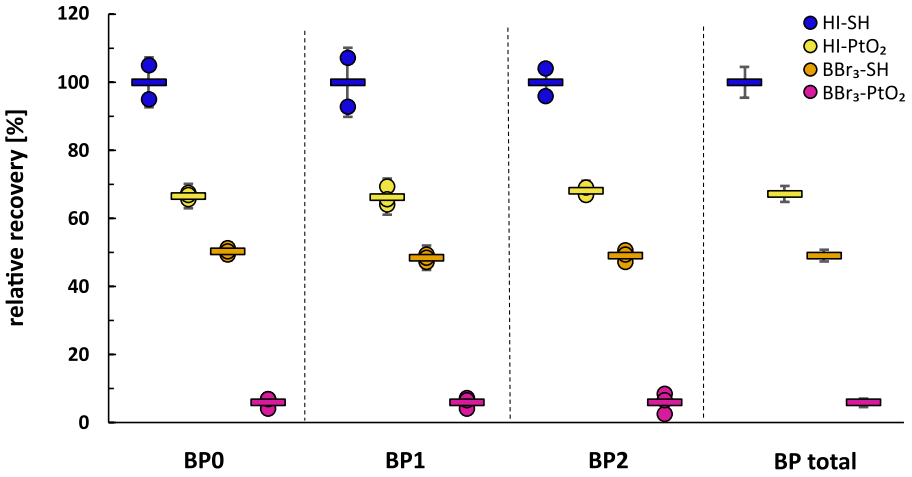

Fig. 3. Relative recovery [%] of BP0, BP1, BP2 and total BP for different ether cleavage and hydrogenation method combinations (HI-SH, HI-PtO_2, BBr_3-SH, BBr_3-PtO_2) tested on *S. acidocaldarius* lipid extracts. The relative recovery describes the amount of recovered material in percent relative to the assay with the highest amount of recovered material. Similarly coloured dots display the measured data points of the triplicates of the respective assay and the coloured bar displays the average recovery of the respective replicates. The error bars show the standard deviation of the average recovery and were determined using Gaussian error propagation. "BP total" are calculated values from the averaged recoveries of BP0, BP1 and BP2. All data were normalized to squalane.

relative to other lipids and the GDGT distribution can differ between archaeal species (Oger and Cario, 2013; Schouten et al., 2013).

3.3. Recovery optimization of SH hydrogenation

The results of the SH hydrogenation optimization experiments (Fig. 4; examined using *S. acidocaldarius* biomass) show similar recovery rates despite different reaction conditions. The recovery is displayed as the relative amount of recovered material in percent compared to the assay with the highest amount of recovered material, in this case SH hydrogenation at 60 °C for 19 h, i.e., overnight. However, all assays were in the range of the most efficient assay, with SH hydrogenation at 50 °C (92%) and 80 °C (93%) as the least efficient ones. Since the hydrogenation for 2 h at 60 °C matches the recovery of the 70 °C/2 h condition, the 60 °C/4 h and the 60 °C/19 h assay within uncertainties and since it has been used in several previous studies (Summons et al., 1998; Bradley et al., 2009; Könneke et al., 2012), we recommend to continue using this protocol (60 °C for 2 h) in terms of reproducibility, comparability, sample throughput, and workflow. It may be possible that using even shorter time than 2 h or shorter time with higher temperature provides sufficient yields, which could further increase sample throughput.

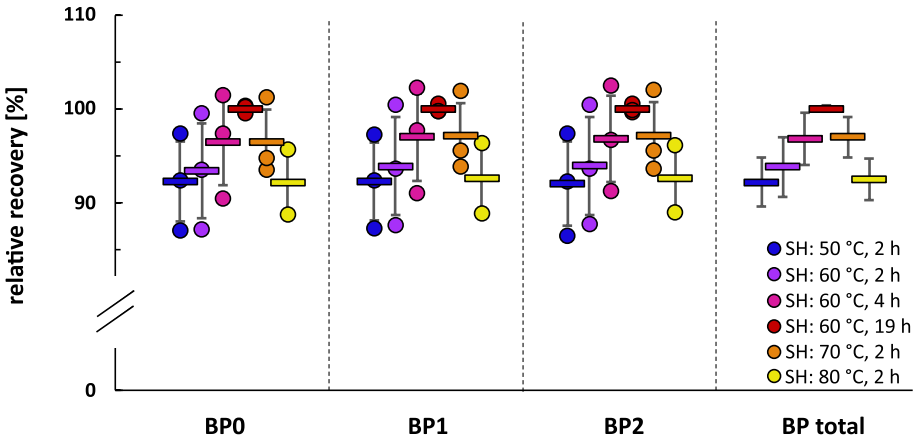

Fig. 4. Relative recovery [%] of BP0, BP1, BP2 and total BP after the hydrogenation with SH of HI-cleaved *S. acidocaldarius* lipid extracts at various reaction conditions. The relative recovery describes the amount of recovered material in percent relative to the assay with the highest amount of recovered material. Dots with same colour display the measured data points of the triplicates of the respective assay and the coloured bar displays the average recovery of the respective replicates. The error bars show the standard deviation of the average recovery and were determined using Gaussian error propagation. "BP total" are calculated values from the averaged recoveries of BP0, BP1 and BP2. All data were normalized to squalane.

3.4. Comparison of stabilized vs. non-stabilized HI

We further investigated the sample recovery during ether cleavage: i) using freshly opened stabilized HI, freshly opened non-stabilized HI, and 5-month-old non-stabilized HI (Fig. 5 A); ii) using 4-months-old HI from the same, formerly freshly opened, batches (Fig. 5 B). It is important to note that the headspace of the HI bottles should be immediately purged with N_2 after each use, the bottles are sealed properly and stored at 4 °C

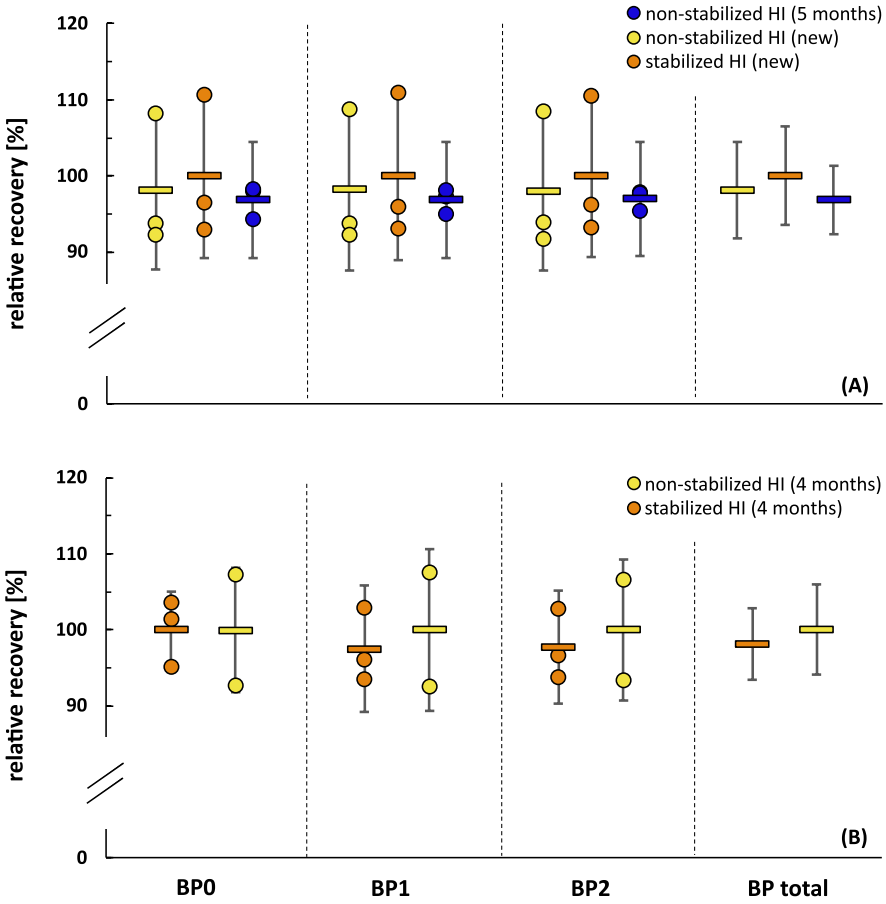

Fig. 5. Relative recovery [%] of BP0, BP1, BP2 and total BP after cleavage and hydrogenation of *S. acidocaldarius* lipid extracts using different types of HI (non-stabilized vs stabilized) and HI of different age. Panel (A) compares freshly opened stabilized HI, freshly opened non-stabilized HI, and 5-month-old non-stabilized HI. Panel (B) compares stabilized HI and non-stabilized HI 4 months after being opened (formerly "freshly opened" HI in panel (A)). The relative recovery describes the amount of recovered material in percent relative to the assay with the highest amount of recovered material. Dots with same colour display the measured data points of the triplicates of the respective assay and the coloured bar displays the average recovery of the respective replicates. The error bars show the standard deviation of the average recovery and were determined using Gaussian error propagation. "BP total" are calculated values from the averaged recoveries of BP0, BP1 and BP2. All data were normalized to squalane.

until the next use. The reaction efficiency of different types and ages of HI was examined using *S. acidocaldarius* biomass. The results are displayed as the relative amount of recovered material in percent compared to the assay with the highest amount of recovered material. Both experiments show similar recovery rates for their assays within their uncertainties. This suggests that the type of HI does not have a significant influence on ether cleavage efficiency, which may be due to the use of HI in excess, which also minimizes the risk of loss of cleavage efficiency due to degradation of the HI, whether it is stabilized or not. However, the stabilization additives for HI could be brand-specific and we have not tested and compared different brands. Nevertheless, we would still recommend using freshly opened HI to minimize any risks of material loss. Although we did not compare absolute yields, the fact that fresh HI has the same relative yield as old HI suggests that the age of HI (within the tested 5-month range) does not impact absolute yields, when used in excess and stored under conditions as inert as possible. The effect of longer storage time or different storage conditions for HI could be addressed in future studies.

3.5. Comparison of the hydrogen isotope fraction during hydrogenation with SH and PtO_2

The results of the SH-PtO_2 comparison with *S. acidocaldarius* and *S. usitatus* after calibration and hydrogenation correction following the approach of Keller et al. (2025) shows that the ether cleavage with HI and subsequent hydrogenation with SH results in initially slightly enriched δ^2H−values (up to +20‰) compared to cleavage and hydrogenation with HI and PtO_2. However, we were able to correct this fractionation effect for *iso*-BPs (biphytanes derived from isoprenoid GDGTs – from *S. acidocaldarius*) resulting in a higher precision of the SH results with an average double standard deviation (2SD) of 3.5‰ compared to PtO_2 with 5.3‰ for *iso*-BP (6.3‰ vs. 9.3‰ for br-C_{30} and 5.0‰ vs. 6.9‰ for br-C_{31}) after all correction steps. The correction of this hydrogen isotope fractionation effect, in the following referred to as Hydrogenation Shift, is explained in detail hereinafter.

The Hydrogenation Shift (HS) for compound class x describes the H-isotope fractionation ($\alpha_{x,HS}$) that occurs from exposure to the hydrogenation agent:

$$\alpha_{x,HS} = \frac{R_{x,after}}{R_{x,before}} = \frac{\delta^2H_{x,after} + 1}{\delta^2H_{x,before} + 1} \quad ; \left[R = \frac{^2H}{^1H}\right] \tag{4}$$

We measured this shift for different readily available compound classes including squalane, alkanes, and our ether-cleavage test compound $C_{18}OC_{18}$ by exposing them to the hydrogenation agents.

The hydrogen isotope fractionation caused by SH treatment seems to differ depending on the type of compound. This non-uniform isotope fractionation effect was supported by the results of the compound comparison using $C_{18}OC_{18}$, nC_{19}, phytane, squalane and the C_8-C_{40}-alkane standard (Fig. 6). After performing the hydrogenation correction according to Leavitt et al. (2023), the results show that hydrogenation with PtO_2 causes similar fractionation for $C_{18}OC_{18}$, nC_{19}, phytane and squalane, while hydrogenation with SH leads to varying, compound-dependent isotope fractionation, e.g. for squalane up to 10‰. In terms of the biphytanes, the hydrogen isotope fractionation after the hydrogen correction after Leavitt et al. (2023) approximately amounts to +10‰ for *iso*-BPs (from *S. acidocaldarius*) and +20‰ for br-C_{30} and br-C_{31} (derived from branched GDGTs – from *S. usitatus*; Fig. 8). However, by correcting this hydrogen isotope fractionation, i.e. the Hydrogenation Shift (Eq. (4)), based on the assumption that the isotopic fractionation of the spiked squalane standard follows the same pathway as the fractionation of the sample, the average hydrogen isotopic composition of *iso*-BPs hydrogenated with SH equals the composition of the *iso*-BPs hydrogenated with PtO_2 (Fig. 8). The isotopic fractionation induced to br-C_{30} and br-C_{31} cannot be resolved entirely by this correction approach, probably due to bigger differences in their chemical structure compared to the squalane standard.

To evaluate the isotopic composition of the added H (δ^2H_{added}) during hydrogenation of alkyl iodides, we measure the original test compound ($C_{18}OC_{18}$) before ether cleavage and hydrogenation and afterwards and use mass balance and the shift fractionation measured above to estimate the hydrogenation added H:

$$nH_{x,after} \cdot R_{x,after} = \alpha_{x,HS} \cdot \left[\left(nH_{x,after} - nH_{added}\right) \cdot R_{x,before} + nH_{added} \cdot R_{added}\right]$$

$$\rightarrow \delta^2H_{added} = \left[\frac{nH_{x,after}}{nH_{added}} \cdot \frac{\delta^2H_{x,after} + 1}{\alpha_{x,HS}} - \left(\frac{nH_{x,after}}{nH_{added}} - 1\right) \cdot \left(\delta^2H_{x,before} + 1\right)\right] - 1 \tag{5}$$

The inferred isotopic composition of the added H (δ^2H_{added}) is listed below. The errors are relatively large because small errors are amplified from estimating the mean value of the isotopic composition of a single H

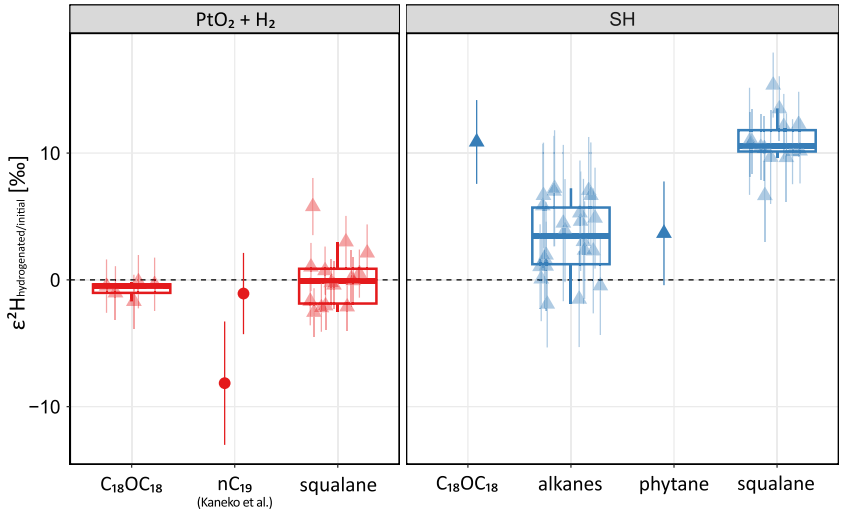

Fig. 6. Hydrogenation Shift, displayed as $\varepsilon^2H_{hydrogenated/initial}$ in ‰, depending on the type of compound and the hydrogenation method, including two data points (circular) from Kaneko et al. (2011). Hydrogenation with $PtO_2 + H_2$ is displayed in red and hydrogenation with SH in blue. The triangular data points display single replicates of the respective compound. (For interpretation of the references to colour in this figure legend, the reader is referred to the web version of this article.)

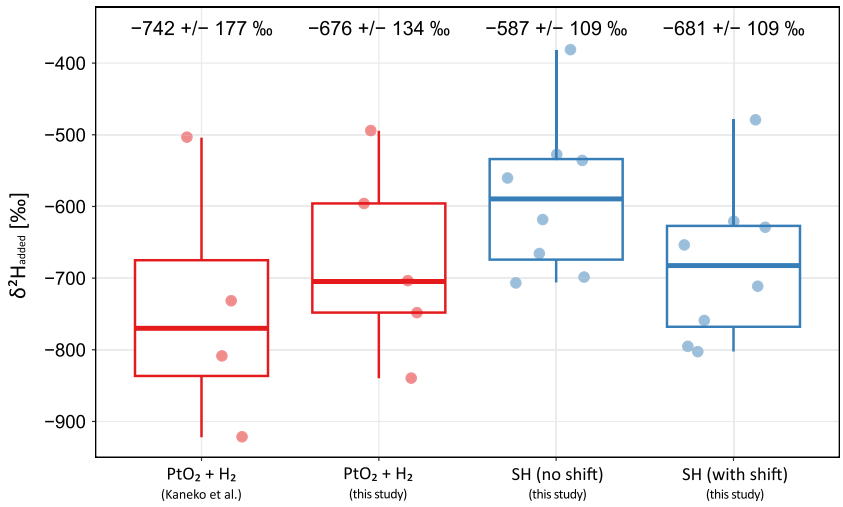

Fig. 7. Estimated isotopic composition δ^2H of the added H (alias δ^2H_{added}) during the hydrogenation of the alkyl iodides depending on the hydrogenation method, including 4 data points from Kaneko et al. (2011). Hydrogenation with $PtO_2 + H_2$ is displayed in red and hydrogenation with SH in blue. The estimated isotopic composition of the added δ^2H during hydrogenation with SH is displayed once without SH correction and (no shift) and once with SH correction (with shift). The circular data points display single replicates of the respective compound. (For interpretation of the references to colour in this figure legend, the reader is referred to the web version of this article.)

out of 38 in the $C_{18}OC_{18}$ derived ether-cleavage and hydrogenation product (C_{18} alkane).

The isotopic composition of the analytes (e.g. biphytanes) can be calculated from the same mass balance (see Eq. (6)) with the measured isotopic composition, the δ^2H_{added} (Table 4, Fig. 7), and the appropriate shift fractionation ($\alpha_{HS} = 1$ if there is no shift, Table 3, Fig. 6):

$$\delta^2H_{analyte} = \left[\frac{nH_{analyte}}{nH_{analyte} - nH_{added}} \cdot \frac{\delta^2H_{analyte.measured} + 1}{\alpha_{analyte.HS}} - \frac{nH_{added}}{nH_{analyte} - nH_{added}} \cdot \left(\delta^2H_{added} + 1\right)\right] - 1 \quad (6)$$

Since the hydrogen isotope fractionation caused by SH is very consistent for the respective compound, also with aged SH (Supplementary information: Fig. S1), of at least up to 5 months, we recommend using SH for the hydrogenation of *iso*-BPs, as a significantly higher sample recovery can be achieved (Section 3.3). Due to the low abundance of isoprenoid GDGTs in many natural samples and technical restrictions in the hydrogen isotope analysis of *iso*-BPs an optimal sample recovery is essential to make hydrogen isotope composition analyses of GDGTs feasible as a paleoenvironmental proxy. With current GC-P-IRMS methods, a minimal sample amount of ca. 150 ng per biphytane is necessary in order to ensure reliable measurements of the hydrogen isotopic composition. Furthermore, the advantages in the handling of SH in contrast to the PtO_2 hydrogenation minimizes the risk of divergences of the reaction times and eliminates the risk of forming explosive gas mixtures with continuous flow of H_2.

In contrast, isotopic fractionation by PtO_2 hydrogenation appears to be slightly less consistent (Fig. 8) as the replicates show lower precision resulting in higher 2SD – in terms of *iso*-BP 5.2‰ compared to SH with 3.5‰ after calibration and 5.3‰ compared to 3.5‰ after all correction steps. This could be caused probably by varying δ^2H of different H_2 batches for hydrogenation and analyses over time, varying PtO_2 particle sizes and surface areas with different batches and varying drying times of the samples in the course of the H_2 bubbling. The consistency of the drying times during H_2 bubbling could probably be improved by developing an experimental setup with pressure distribution control units and different sample vial and cap sizes and types, but that does not eliminate the problem of varying H_2 batches and the absent control of the PtO_2 properties as well as the handling risks of H_2. However, in terms of biomarkers other than isoprenoid GDGTs, e.g., branched GDGTs, we recommend ether cleavage with HI at 120 °C for 4 h but with subsequent hydrogenation with PtO_2 and H_2 gassing, as it was not possible to implement a reliable SH correction for these biomarkers. We therefore recommend accepting the loss of sample material (See section 3.3) and slightly higher isotopic composition uncertainties (Fig. 8) in exchange for a correct δ^2H until the SH method and the correction protocol are further improved.

Table 3
Overview of the Hydrogenation Shift, displayed as $\varepsilon^2H_{hydrogenated/initial}$, alias ε^2H, of different compounds depending on the hydrogenation method.

hydrogenation	sample type	replicates	analyses	mean ε^2H [‰]	ε^2H uncertainty [‰]
Pt/H_2	$C_{18}OC_{18}$	5	36	−0.74	2.10
Pt/H_2	squalane	15	71	0.13	2.26
SH	squalane	14	63	10.91	2.91
SH	$C_{18}OC_{18}$	1	10	10.56	3.31
SH	Alkanes (22)	1	69	3.33	4.17
SH	phytane	1	7	4.90	4.09

Table 4
Estimated isotopic composition of added H (alias δ^2H_{added}) during hydrogenation of alkyl iodides.

study	hydrogenation	shift correction	replicates	analyses	δ^2H_{added} mean [‰]	uncertainty [‰]
this study	Pt/H_2	no	5	36	−676.43	134.33
this study	SH	no	8	50	−586.77	108.79
this study	SH	with	8	50	−681.21	108.57
Kaneko et al.	Pt/H_2	no	4	14	−741.50	176.54

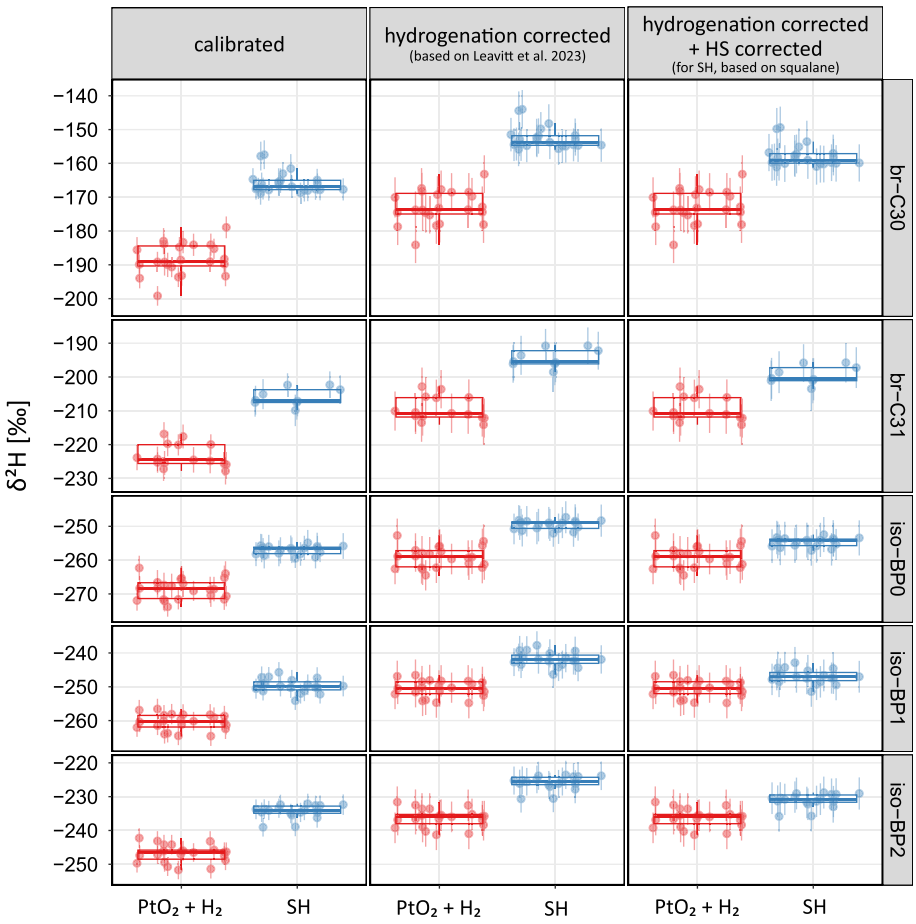

Fig. 8. Comparison of δ^2H in ‰ of br-C_{30} and br-C_{31} (derived from *S. usitatus*) and *iso*-BPs (derived from *S. acidocaldarius*) depending the hydrogenation method and three different correction steps: (I) calibrated ("calibrated"); (II) calibrated and hydrogenation corrected ("hydrogenation corrected") based on Leavitt et al. (2023); and (III) calibrated, hydrogenation corrected and Hydrogenation Shift (HS) corrected in terms of the SH data ("hydrogenation corrected + HS corrected"). Hydrogenation with $PtO_2 + H_2$ is displayed in red and hydrogenation with SH in blue. The circular data points display single replicates of the respective compound. (For interpretation of the references to colour in this figure legend, the reader is referred to the web version of this article.)

4. Conclusions

Based on optimal efficiency and minimized hydrogen isotopic fractionation, we recommend for archaeal GDGTs ether cleavage with HI at 120 °C for 4 h followed by hydrogenation with SH at 60 °C for 2 h. Using this method, a high sample recovery can be achieved, with low, but consistent and reliably correctable, hydrogen isotopic fractionation while ensuring the comparability to previous studies using SH. An optimal sample recovery is important due to the low abundance of isoprenoid GDGTs in many natural samples and, to this date, a minimal sample amount of ca. 150 ng per biphytane in order to ensure reliable analysis of the hydrogen isotopic composition.

In terms of other biomarkers e.g., branched GDGTs, we also recommend ether cleavage with HI at 120 °C for 4 h but with subsequent hydrogenation with PtO_2 and H_2 gassing. This combination has a lower sample recovery (See section 3.3) and slightly higher isotopic uncertainties, but it was not yet possible to implement a reliable SH correction for these compounds due to the lack of a suitable standard. In exchange for a correct hydrogen isotopic composition, we recommend hydrogenation with PtO_2 and H_2 gassing for these biomarkers until the SH method and the correction protocol are further improved.

The HI comparison test (See section 3.4) emphasizes that the excess usage of HI can avoid possible loss of cleavage efficiency due to degradation of HI with age. Although the test did not show significant differences between stabilized or non-stabilized and freshly opened and aged HI, we recommend using freshly opened HI to minimize any risks. The SH assay (See section 3.3) shows that small improvements of the recovery might be possible by using a higher reaction temperature, if necessary, but higher reaction temperatures might increase the risk of material loss and increase handling risks in case of leakages as the SH liquid and resulting vapour are highly inflammable. More testing at higher temperatures, with shorter reaction times and different glass vial and cap combinations to improve the sealing and minimize material loss would be required. Deviating hydrogenation conditions might require a revision of the SH Hydrogenation Shift correction, which was developed for hydrogenation with SH at 60 °C for 2 h. Similarly, different reaction times and potentially lower temperatures could be tested for the $PtO_2 + H_2$ method, while temperatures higher than room temperature are not advisable due to safety issues concerning H_2. Additionally, it is important to note that environmental samples may have a more complex molecular composition than the cultures and standards used in this study, which could affect cleavage and hydrogenation efficiencies due to matrix effects. These potential matrix effects should be addressed in future studies.

The improvement of these ether cleavage and hydrogenation protocols represents an important step in the further development of hydrogen isotope composition analyses of GDGTs as a possible paleoenvironmental proxy and will improve the comparability of potential paleorecords of δ^2H of GDGTs in this research field.

CRediT authorship contribution statement

C.D. Rosendahl: Writing – original draft, Visualization, Validation, Methodology, Investigation, Funding acquisition, Formal analysis, Data curation, Conceptualization. **X. Zhao:** Writing – review & editing, Validation, Methodology, Formal analysis, Data curation. **A.E. Maloney:** Writing – review & editing, Validation, Methodology, Investigation, Formal analysis, Data curation. **J.M. McFarlin:** Writing – review & editing, Validation, Methodology, Investigation, Formal analysis, Data curation, Conceptualization. **K.J. Keller:** Writing – review & editing, Validation, Methodology, Investigation, Formal analysis, Data curation, Conceptualization. **R. Kreutz:** Writing – review & editing, Methodology, Investigation, Data curation. **J. Altun:** Writing – review & editing, Methodology, Investigation, Data curation. **L.H. Bachmann:** Writing – review & editing, Methodology, Investigation, Data curation. **J. Hartmann:** Writing – review & editing, Methodology, Investigation, Data curation. **H.K. Batther:** Writing – review & editing, Methodology, Investigation, Data curation. **A.N. Calhoun:** Writing – review & editing, Methodology, Investigation, Data curation. **M. Elvert:** Writing – review & editing, Supervision, Resources, Methodology. **A. Pearson:** Writing – review & editing, Supervision, Resources, Conceptualization. **W.D. Leavitt:** Writing – review & editing, Validation, Methodology, Formal analysis, Data curation, Conceptualization. **S.H. Kopf:** Writing – review & editing, Visualization, Validation, Supervision, Software, Resources, Methodology, Investigation, Formal analysis, Data curation, Conceptualization. **F.J. Elling:** Writing – review & editing, Validation, Supervision, Resources, Project administration, Funding acquisition, Formal analysis, Data curation, Conceptualization.

Declaration of competing interest

The authors declare that they have no known competing financial interests or personal relationships that could have appeared to influence the work reported in this paper.

Acknowledgements

Funding for this work was provided by the Deutsche Forschungsgemeinschaft (grant # 441217575, to FJE) and the European Association of Organic Geochemists through an EAOG Research Award (to CDR). Research at Harvard University was funded by the American Chemical Society (ACS-PRF grant #66614-ND2, to AP). We acknowledge the analytical contributions of the CU Boulder Earth Systems Stable Isotope Lab (CUBES-SIL) Core Facility (RRID:SCR_019300). We also thank Thomas Blanz and Silvia Koch for access to GC-FID at Kiel University and Enno Schefuß for access to GC-FID at MARUM-Center for Marine Environmental Sciences, University of Bremen. The authors also thank the anonymous reviewers for their careful evaluations and constructive comments.

Appendix A. Supplementary data

Supplementary data to this article can be found online at https://doi.org/10.1016/j.orggeochem.2026.105139.

Data availability

The data underlying this study are available in the published article and its online supplementary material.

References

Blewett, J., Elling, F.J., Naafs, B.D.A., Kattein, L., Evans, T.W., Lauretano, V., Gallego-Sala, A.V., Pancost, R.D., Pearson, A., 2022. Metabolic and ecological controls on the stable carbon isotopic composition of archaeal (isoGDGT and BDGT) and bacterial (brGDGT) lipids in wetlands and lignites. Geochimica et Cosmochimica Acta 320, 1–25. https://doi.org/10.1016/j.gca.2021.12.023.

Bradley, A.S., Hayes, J.M., Summons, R.E., 2009. Extraordinary 13C enrichment of diether lipids at the lost city Hydrothermal field indicates a carbon-limited ecosystem. Geochimica et Cosmochimica Acta 73, 102–118. https://doi.org/10.1016/j.gca.2008.10.005.

Colcord, D.E., Pearson, A., Brassell, S.C., 2017. Carbon isotopic composition of intact branched GDGT core lipids in Greenland lake sediments and soils. Organic Geochemistry 110, 25–32. https://doi.org/10.1016/j.orggeochem.2017.04.008.

Dirghangi, S.S., Pagani, M., 2013. Hydrogen isotope fractionation during lipid biosynthesis by *Haloarcula marismortui*. Geochimica et Cosmochimica Acta 119, 381–390. https://doi.org/10.1016/j.gca.2013.05.023.

Elling, F.J., Kattein, L., Naafs, B.D.A., Lauretano, V., Pearson, A., 2023. Heterotrophic origin and diverse sources of branched glycerol monoalkyl glycerol tetraethers (brGMGTs) in peats and lignites. Organic Geochemistry 178, 104558. https://doi.org/10.1016/j.orggeochem.2023.104558.

Guan, H., Feng, D., Wu, N., Chen, D., 2016. Methane seepage intensities traced by biomarker patterns in authigenic carbonates from the South China Sea. Organic Geochemistry 91, 109–119. https://doi.org/10.1016/j.orggeochem.2015.11.007.

Harris, C.M., Kopf, S., Rhim, J.H., Cobban, A., Elling, F.J., Feng, X., McFarlin, J., Weber, Y., Zhang, Y., Zhou, A., Batther, H., Pearson, A., Leavitt, W.D., 2025. Lipid hydrogen isotope compositions primarily reflect growth water in the model archaeon *Sulfolobus acidocaldarius*. Applied and Environmental Microbiology 91, e01983–e02024. https://doi.org/10.1128/aem.01983-24.

He, J., Jia, J., Guo, W., Jia, G., 2022. Archaeal tetraether lipids and their biphytane carbon isotope composition in sediments along an estuarine biogeochemical gradient. Geochimica et Cosmochimica Acta 318, 452–467. https://doi.org/10.1016/j.gca.2021.12.015.

Hoefs, M., Schouten, S., De Leeuw, J.W., King, L.L., Wakeham, S.G., Sinninghe Damsté, J. S., 1997. Ether lipids of planktonic archaea in the marine water column. Applied and Environmental Microbiology 63, 3090–3095. https://doi.org/10.1128/aem.63.8.3090-3095.1997.

Hurley, S.J., Close, H.G., Elling, F.J., Jasper, C.E., Gospodinova, K., McNichol, A.P., Pearson, A., 2019. CO_2-dependent carbon isotope fractionation in Archaea, Part II: the marine water column. Geochimica et Cosmochimica Acta 261, 383–395. https://doi.org/10.1016/j.gca.2019.06.043.

Husa, W.J., Shattuck, P.S., 1932. The effect of various iodides upon the stability of hydriodic acid. The Journal of the American Pharmaceutical Association 1912, 114–121. https://doi.org/10.1002/jps.3080210205.

Jahn, U., Summons, R., Sturt, H., Grosjean, E., Huber, H., 2004. Composition of the lipids of *Nanoarchaeum equitans* and their origin from its host Ignicoccus sp. strain KIN4/I. Archives of Microbiology 182, 404–413. https://doi.org/10.1007/s00203-004-0725-x.

Kaneko, M., Kitajima, F., Naraoka, H., 2011. Stable hydrogen isotope measurement of archaeal ether-bound hydrocarbons. Organic Geochemistry 42, 166–172. https://doi.org/10.1016/j.orggeochem.2010.11.002.

Keller, K., Kopf, S., McFarlin, J., Maloney, A., Rhim, J.H., Elling, F.J., Ashing-Giwa, K., Baker, I., Calhoun, A., Pearson, A., 2025a. Compound-specific carbon and hydrogen isotope analysis traces archaeal lipid signatures in cold seep marine systems. Geochimica et Cosmochimica Acta 407, 309–321. https://doi.org/10.1016/j.gca.2025.08.017.

Keller, K., Baum, M.M., Liu, X.-L., Ashing-Giwa, K., Baker, I.R., Blewett, J., Pearson, A., 2025b. Constraining the sources of archaeal tetraether lipids in multiple cold seep provinces of the Cascadia Margin. Organic Geochemistry 200, 104882. https://doi.org/10.1016/j.orggeochem.2024.104882.

Könneke, M., Lipp, J.S., Hinrichs, K.-U., 2012. Carbon isotope fractionation by the marine ammonia-oxidizing archaeon *Nitrosopumilus maritimus*. Organic Geochemistry 48, 21–24. https://doi.org/10.1016/j.orggeochem.2012.04.007.

Kuypers, M.M.M., Blokker, P., Erbacher, J., Kinkel, H., Pancost, R.D., Schouten, S., Sinninghe Damsté, J.S., 2001. Massive expansion of marine archaea during a mid-cretaceous oceanic anoxic event. Science 293, 92–95. https://doi.org/10.1126/science.1058424.

Leavitt, W.D., Kopf, S.H., Weber, Y., Chiu, B., McFarlin, J.M., Elling, F.J., Hoeft-McCann, S., Pearson, A., 2023. Controls on the hydrogen isotope composition of tetraether lipids in an autotrophic ammonia-oxidizing marine archaeon. Geochimica et Cosmochimica Acta 352, 194–210. https://doi.org/10.1016/j.gca.2023.04.033.

Lengger, S.K., Lipsewers, Y.A., De Haas, H., Sinninghe Damsté, J.S., Schouten, S., 2014. Lack of ^{13}C-label incorporation suggests low turnover rates of thaumarchaeal intact polar tetraether lipids in sediments from the Iceland shelf. Biogeosciences 11, 201–216. https://doi.org/10.5194/bg-11-201-2014.

Lengger, S.K., Weber, Y., Taylor, K.W.R., Kopf, S.H., Berstan, R., Bull, I.D., Mayser, J.-P., Leavitt, W.D., Blewett, J., Pearson, A., Pancost, R.D., 2021. Determination of the δ^2H values of high molecular weight lipids by high-temperature gas chromatography coupled to isotope ratio mass spectrometry. Rapid Communications in Mass Spectrometry 35, e8983. https://doi.org/10.1002/rcm.8983.

Liu, X.-L., De Santiago Torio, A., Bosak, T., Summons, R.E., 2016. Novel archaeal tetraether lipids with a cyclohexyl ring identified in Fayetteville Green Lake, NY, and other sulfidic lacustrine settings. Rapid Communications in Mass Spectrometry 30, 1197–1205. https://doi.org/10.1002/rcm.7549.

Liu, X.-L., Lipp, J.S., Simpson, J.H., Lin, Y.-S., Summons, R.E., Hinrichs, K.-U., 2012. Mono- and dihydroxyl glycerol dibiphytanyl glycerol tetraethers in marine sediments: Identification of both core and intact polar lipid forms. Geochimica et Cosmochimica Acta 89, 102–115. https://doi.org/10.1016/j.gca.2012.04.053.

Oger, P.M., Cario, A., 2013. Adaptation of the membrane in Archaea. Biophysical Chemistry, Biomolecular Systems under Extreme Environmental Conditions 183, 42–56. https://doi.org/10.1016/j.bpc.2013.06.020.

Oren, A., Garrity, G.M., 2021. Valid publication of the names of forty-two phyla of prokaryotes. International Journal of Systematic and Evolutionary Microbiology 71, 005056. https://doi.org/10.1099/ijsem.0.005056.

Pancost, R.D., van Geel, B., Baas, M., Sinninghe Damsté, J.S., 2000. $\delta^{13}C$ values and radiocarbon dates of microbial biomarkers as tracers for carbon recycling in peat deposits. Geology 28, 663–666. https://doi.org/10.1130/0091-7613(2000)28%253C663:CVARDO%253E2.0.CO;2.

Pearson, A., Huang, Z., Ingalls, A.E., Romanek, C.S., Wiegel, J., Freeman, K.H., Smittenberg, R.H., Zhang, C.L., 2004. Nonmarine crenarchaeol in nevada hot springs. Applied and Environmental Microbiology. https://doi.org/10.1128/AEM.70.9.5229-5237.2004.

Pearson, A., Hurley, S.J., Elling, F.J., Wilkes, E.B., 2019. CO_2-dependent carbon isotope fractionation in Archaea, Part I: Modeling the 3HP/4HB pathway. Geochimica et Cosmochimica Acta 261, 368–382. https://doi.org/10.1016/j.gca.2019.06.042.

Pearson, A., Hurley, S.J., Walter, S.R.S., Kusch, S., Lichtin, S., Zhang, Y.G., 2016. Stable carbon isotope ratios of intact GDGTs indicate heterogeneous sources to marine sediments. Geochimica et Cosmochimica Acta 181, 18–35. https://doi.org/10.1016/j.gca.2016.02.034.

Polik, C.A., Elling, F.J., Pearson, A., 2018. Impacts of paleoecology on the TEX86 sea surface temperature proxy in the pliocene-pleistocene mediterranean sea. Paleoceanography and Paleoclimatology 33, 1472–1489. https://doi.org/10.1029/2018PA003494.

Polissar, P.J., D'Andrea, W.J., 2014. Uncertainty in paleohydrologic reconstructions from molecular δD values. Geochimica et Cosmochimica Acta 129, 146–156. https://doi.org/10.1016/j.gca.2013.12.021.

Rhim, J., Kopf, S., McFarlin, J., Maloney, A., Batther, H., Harris, C., Zhou, A., Feng, X., Weber, Y., Hoeft-McCann, S., Pearson, A., Leavitt, W., 2023. Metabolic imprints in the hydrogen isotopes of *Archaeoglobus fulgidus*tetraether lipid. Doi: 10.1101/2023.11.29.569324.

Schouten, S., Hopmans, E.C., Sinninghe Damsté, J.S., 2013. The organic geochemistry of glycerol dialkyl glycerol tetraether lipids: a review. Organic Geochemistry 54, 19–61. https://doi.org/10.1016/j.orggeochem.2012.09.006.

Summons, R.E., Franzmann, P.D., Nichols, P.D., 1998. Carbon isotopic fractionation associated with methylotrophic methanogenesis. Organic Geochemistry 28, 465–475. https://doi.org/10.1016/S0146-6380(98)00011-4.

Weber, Y., Sinninghe Damsté, J.S., Zopfi, J., De Jonge, C., Gilli, A., Schubert, C.J., Lepori, F., Lehmann, M.F., Niemann, H., 2018. Redox-dependent niche differentiation provides evidence for multiple bacterial sources of glycerol tetraether lipids in lakes. Proceedings of the National Academy of Sciences 115, 10926–10931. https://doi.org/10.1073/pnas.1805186115.

Weijers, J.W.H., Wiesenberg, G.L.B., Bol, R., Hopmans, E.C., Pancost, R.D., 2010. Carbon isotopic composition of branched tetraether membrane lipids in soils suggest a rapid turnover and a heterotrophic life style of their source organism(s). Biogeosciences 7, 2959–2973. https://doi.org/10.5194/bg-7-2959-2010.

Zhang, Y.G., Zhang, C.L., Liu, X.-L., Li, L., Hinrichs, K.-U., Noakes, J.E., 2011. Methane Index: a tetraether archaeal lipid biomarker indicator for detecting the instability of marine gas hydrates. Earth and Planetary Science Letters 307, 525–534. https://doi.org/10.1016/j.epsl.2011.05.031.

Zhu, Q.-Z., Elvert, M., Meador, T.B., Schröder, J.M., Doeana, K.D., Becker, K.W., Elling, F.J., Lipp, J.S., Heuer, V.B., Zabel, M., Hinrichs, K.-U., 2024. Comprehensive molecular-isotopic characterization of archaeal lipids in the Black Sea water column and underlying sediments. Geobiology 22, e12589. https://doi.org/10.1111/gbi.12589.